ISSN 0915-633X

NATIONAL INSTITUTE FOR FUSION SCIENCE

Modelling of Density Limit Phenomena in Toroidal Helical Plasmas

K. Itoh, S.-I. Itoh and L. Giannone

(Received - Feb. 17, 2000)

NIFS-627 Mar. 2000

RESEARCH REPORT
NIFS Series

NAGOYA, JAPAN

Modelling of Density Limit Phenomena in Toroidal Helical Plasmas

K. Itoh[1], S.-I. Itoh[2], L. Giannone[3]

[1] *National Institute for Fusion Studies, Toki 509-5292, Japan.*

[2] *Research Institute for Applied Mechanics, Kyushu University, Kasuga 816-8580 Japan.*

[3] *Max Planck Institut für Plasmaphysik, EURATOM-IPP Association, D-85748 Garching, FRG*

Abstract

The physics of density limit phenomena in toroidal helical plasmas based on an analytic point model of toroidal plasmas is discussed. The combined mechanism of the transport and radiation loss of energy is analyzed, and the achievable density is derived. A scaling law of the density limit is discussed. The dependence of the critical density on the heating power, magnetic field, plasma size and safety factor in the case of L-mode energy confinement is explained. The dynamic evolution of the plasma energy and radiation loss is discussed. Assuming a simple model of density evolution, of a sudden loss of density if the temperature becomes lower than critical value, then a limit cycle oscillation is shown to occur. A condition that divides the limit cycle oscillation and the complete radiation collapse is discussed. This model seems to explain the density limit oscillation that has been observed on the W7-AS stellarator.

keywords: density limit, radiation loss, anomalous transport, L-mode scaling law, helical systems

1. Introduction

Recently, much attention has been paid to the density limit phenomena in toroidal helical plasmas [1-8]. The physics phenomenon, which occurs in the vicinity of the operational density limit, has various aspects of importance. Firstly, this process is considered to dictate the achievable plasma performance. The lack of toroidal symmetry could cause the enhancement of the energy loss in the long mean free path regime, and the anomalous transport also tends to increase (in the absence of the transition to an improved confinement state) if the plasma temperature increases. Therefore the optimum fusion triplet, which is the product of density, ion temperature and confinement time, is expected in the high density regime. The density limit could impose an upper bound on the fusion triplet value. Secondly, in the W7-AS stellarator the H-mode, the most typical example of the improved confinement modes, occurs when the density becomes higher than the critical density for transition. Empirically, this critical density for the H-mode transition is known to become larger as the heating

power increases [9]. The knowledge of the operational density limit is necessary to establish the perspective for the realization of the H-mode with high heating power. Thirdly, plasmas in toroidal helical devices are operated mainly in a condition which are free from current-driven global MHD instabilities. Owing to this fact, precise experimental studies could be performed in toroidal helical plasmas even in the final phase of the radiation collapse. An attractive research area has been identified.

One important mechanism associated with the density limit phenomena is considered to be the radiation loss of line emission from impurity ions. The radiation loss can have a temperature dependence such that the loss increases if the temperature decreases [10]. Owing to this dependence, the radiation loss could cause the radiation collapse of plasma discharge in a similar fashion to detachment or MARFE formation [11]. A large scale deformation of the temperature profile often causes current disruption or strong degradation of confinement in tokamaks. This limit has been called the density limit in tokamaks [12]. The dynamics of radiation collapse also depends on the impurity species. When a heavy impurity like tungsten plays a dominant role, plasma with strongly hollow electron temperature profile is formed [13].

In toroidal helical devices the current disruption might not take place but a strong degradation of confinement occurs if radiation collapse happens. The transport of impurities in helical plasmas has been studied intensively [14, 15]. The limit of density due to radiation collapse has been studied and the dependence of the critical density on the plasma heating power was derived [1]. An empirical scaling law for the density limit in helical devices has been presented and a dependency on the magnetic field has become clear [2, 8]. In addition, a periodic oscillation of the plasma energy in the vicinity of the density limit on LHD, CHS and W7-AS devices [5-8, 16] has been found recently. Such dynamics attract special interest because it is a characteristic example of self-sustained oscillation in confined plasmas.

In this article, we discuss the physics of the density limit phenomena based on an analytic model of toroidal helical plasmas. The combination of the transport loss of energy and radiation loss is analyzed and the scaling law for the density limit is derived. The parameter dependence of the critical density is explained. In the case of L-mode confinement, an approximate relation like $n_c \sim P^{1/2} B^{1/2} V^{-1/3} q^{-1/4}$ is derived (P : heating power, B : magnetic field, V : plasma volume, q : safety factor). Then, the dynamical evolution of the plasma energy and radiation loss is discussed. By a method of reduction of variables, a simple model equation of the self-generated oscillation near the density limit is presented. A mechanism of density clump (i.e., rapid decay of density) at low plasma temperature is presented. A condition for the oscillation to occur when the density exceeds the density limit is derived.

2. Model of Density Limit

2.1 Point model

We start from the simple energy balance equation

$$\frac{d}{dt}W = -\frac{1}{\tau_E}W - P_{rad} + P \quad (1)$$

where W is the plasma energy, P_{rad} is the radiation loss, P is the heating power, and W/τ_E are the other loss processes. We here consider that τ_E is the energy confinement time governed by the transport processes. In the point model, the radiation loss is expressed as

$$P_{rad} = n_e n_I \left\langle L_Z(T) \right\rangle V \quad (2)$$

where n_e is the averaged electron energy, n_I is the averaged impurity ion density, T is the averaged electron temperature and V is the plasma volume. The radiation rate coefficient L_Z is usually defined as a local value, being a function of the local temperature. In this article, for the transparency of the analysis, we use a volume average value $\left\langle L_Z(T) \right\rangle$. This means that the influence of the profiles of temperature or density is included in the coefficient.

2.2 Stationary Solution

The stationary state is given by the relation

$$P = \frac{1}{\tau_E}W + P_{rad} . \quad (3)$$

Model forms for the radiation loss and transport loss are introduced. The radiation rate coefficient has a dependence on temperature shown schematically in Fig. 1. Above a certain energy, which corresponds to the spectrum edge of impurity ions, it is a decreasing function of the temperature (until the next edge is reached). We therefore choose a simple power law form for the analytical study

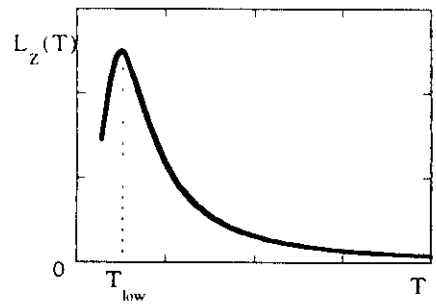

Fig.1 Conceptual drawing of the radiation rate coefficient

$$\left\langle L_Z(T) \right\rangle = \xi T^{-\gamma} \quad (4)$$

in the range $\left(T > T_{low}\right)$. For simplicity, we assume that the lower limiting temperature, T_{low}, is much lower than the temperature which is realized by the balance of the input power and transport loss. The coefficient represents the species of ions and reflects the influence of profiles. By introducing this form of radiation rate coefficient, the radiation loss is expressed as :

$$P_{rad} = n^2 \left(\frac{n_I}{n}\right) \xi T^{-\gamma} V \quad (5)$$

In the following, n denotes the averaged electron density. The confinement time is also expressed in a similar way where the profile effect is included in τ_{E0} as:

$$\tau_E = \tau_{E0} n^{\beta} T^{-\alpha} \quad (6)$$

The dependence of the density and temperature is explicitly separated, in order to illustrate the

dependence of the total loss on the density and temperature. The transport loss of energy is expressed as ($W = 3nTV$, assuming that $T_e = T_i$)

$$\frac{1}{\tau_E} W = \frac{3V}{\tau_{E0}} n^{1-\beta} T^{1+\alpha} \qquad (7)$$

From Eqs.(5) and (7), the equation for the stationary state, Eq(3), is written as

$$P = \frac{3V}{\tau_{E0}} n^{1-\beta} T^{1+\alpha} + V\left(\frac{n_I}{n}\right) \xi n^2 T^{-\gamma} . \quad (8)$$

Equation (8) describes the relation between the plasma temperature and density under the given heating power P . Figure 2 illustrates the relation between T and n . Equation (8) describes the accessible region of the density for the given heating power. The accessible density region is calculated from the total energy loss rate. The dependence of the total loss (i.e., the right hand side of Eq.(8), $P_{tot} = P_{trans} + P_{rad}$) on the temperature is studied. The loss P_{tot} has an asymptotic form of $T^{-\gamma}$

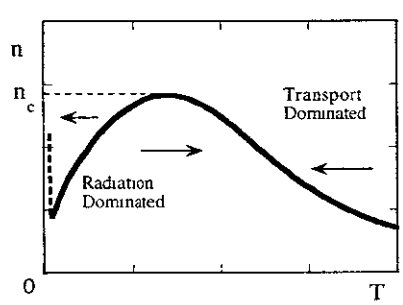

Fig.2 Energy balance curve which satisfies Eq.(8) for a given power. There is an upper bound of density, above which the stationary solution does not exist. The curve in the region $T < T_{low}$ is plotted by dotted line. Arrows indicates the direction of temperature evolution when the stationary condition is not satisfied.

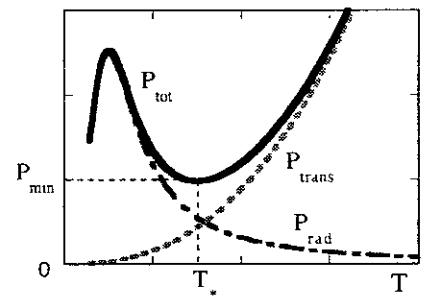

Fig.3 Loss power is shown as a function of temperature for the fixed density. Total loss has a minimum at $T = T_*$.

in the low temperature limit and $T^{1+\alpha}$ in the high temperature limit. The right hand side of Eq.(8) increases both in the low and high temperature limits as is shown in Fig.3. It has the minimum value at the temperature T_* ,

$$P \geq P_{min} \qquad (9)$$

$$P_{min} = C\, V \left(\frac{n_I}{n}\right)^{1/(1+\mu)} \xi^{1/(1+\mu)}\, \tau_{E0}^{-\mu/(1+\mu)} n^{(2+\mu-\beta\mu)/(1+\mu)} \qquad (10)$$

where the abbreviation is made as

$$\mu = \frac{\gamma}{1+\alpha} \qquad (11)$$

and the numerical coefficient C is given by $C = (1+\mu)(\mu/3)^{-\mu/(1+\mu)}$. The temperature T_* is given by:

$$T_* = \left\{ \frac{\mu}{3} \left(\frac{n_I}{n}\right) \xi\, \tau_{E0} n^{1+\beta} \right\}^{1/(1+\alpha+\gamma)} . \qquad (12)$$

At the condition of minimum loss, the relation

$$P_{rad} = \frac{1}{\mu} P_{trans} \qquad (13)$$

holds.

2.3 Density Limit

Equation (10) describes the minimum and necessary heating power in order to realize the stationary solution in the presence of the radiation loss and the transport loss. The minimum value $P_{\min}(n)$ is a function of the density. The condition, $P \geq P_{\min}(n)$, can be rewritten as

$$n \leq n_c \qquad (14)$$

where the upper bound of the density is explicitly given as

$$n_c = C' V^{-(1+\mu)/(2+\mu-\beta\mu)} \left(\frac{n_I}{n}\right)^{-1/(2+\mu-\beta\mu)} \times \xi^{-1/(2+\mu-\beta\mu)} \tau_{E0}^{\mu/(2+\mu-\beta\mu)} P^{(1+\mu)/(2+\mu-\beta\mu)} \qquad (15)$$

In this expression, the numerical coefficient C' is given as $C' = C^{-(1+\mu)/(2+\mu-\beta\mu)}$.

Equation (15) shows that various quantities dictate the upper bound of the density. We here introduce the separation of the critical density into two factors as

$$n_c = f_{cI} \cdot f_{cT} \qquad (16)$$

where

$$f_{cI} = C' \left(\frac{n_I}{n}\right)^{-1/(2+\mu-\beta\mu)} \xi^{-1/(2+\mu-\beta\mu)} \qquad (17)$$

and

$$f_{cT} = V^{-(1+\mu)/(2+\mu-\beta\mu)} \tau_{E0}^{\mu/(2+\mu-\beta\mu)} P^{(1+\mu)/(2+\mu-\beta\mu)} . \qquad (18)$$

The factor f_{cI} comes from the specification concerning on the impurity ions (relative abundance, species or profile, etc), and f_{cT} represents the impact of energy transport.

The critical density in Eq.(15) is defined such that the stationary equilibrium disappears above this critical density for other fixed parameters. The gradual degradation of energy confinement could occur when the density comes closer to the critical density. At this critical density, $n = n_c$, Eq.(13) holds, so that the transport loss is reduced from the total input power as $P_{trans} = \mu P/(1+\mu)$. The total plasma energy, $W = \tau_E P_{trans}$, satisfies the relation

$$\frac{W}{P} = \frac{\mu}{1+\mu} \tau_E \qquad (19)$$

This shows the reduction of global energy confinement, that is the left hand side of Eq.(19), at the critical density.

2.4 Parameter dependence of critical density

By specifying the property of the transport loss, the dependence of the critical density on the plasma parameters is discussed.

The energy confinement time has dependencies on the magnetic field and plasma size, in addition to those on density and temperature. We use a form

$$\tau_E \propto B^{a_2} L^{a_3} q^{-a_4} n^{\beta} T^{-\alpha} \qquad (20)$$

where B is the magnetic field, q is a safety factor (inverse of the rotational transform) and L is the system size,

$$V = L^3 . \qquad (21)$$

The dependence

$$\tau_{E0} \propto B^{a_2} L^{a_3} q^{-a_4} \qquad (22)$$

is substituted in Eq.(18), and the following relation is obtained as

$$f_{cT} \propto P^{c_1} B^{c_2} L^{-c_3} q^{-c_4} \qquad (23)$$

where indices are given as

$$c_1 = \frac{1+\alpha+\gamma}{2+2\alpha+(1-\beta)\gamma} \qquad (24\text{-}1)$$

$$c_2 = \frac{a_2\gamma}{2+2\alpha+(1-\beta)\gamma} \qquad (24\text{-}2)$$

$$c_3 = \frac{3+3\alpha+(3-a_3)\gamma}{2+2\alpha+(1-\beta)\gamma} \qquad (24\text{-}3)$$

and

$$c_4 = \frac{a_4\gamma}{2+2\alpha+(1-\beta)\gamma} \qquad (24\text{-}4)$$

If the properties of impurity radiation are not altered and f_{cl} is considered to be constant, the parameter dependence of the critical density is derived as

$$n_c \propto P^{c_1} B^{c_2} L^{-c_3} q^{-c_4} . \qquad (25)$$

2.5 Case study for transport models

2.5.1 Empirical scaling for confinement time

Studies to correlate the confinement time with the input heating power have been made. Coefficients $(\alpha, \beta, a_2, a_3, a_4)$ are fitted from the empirical scaling law. The empirical dependence on the heating power is interpreted as the dependence on temperature.

In the limit where the transport process dominates the energy loss, $W/\tau_E >> P_{rad}$, the energy balance equation is rewritten as $3nTV = \tau_E P$. Elimination of T from this relation by use of Eq.(4), $\tau_E = \tau_{E0} n^{\beta} T^{-\alpha}$, provides the energy confinement time as a function of heating power as

$$\tau_E = \tau_{E0}^{1/(1+\alpha)} L^{3\alpha/(1+\alpha)} n^{(\alpha+\beta)/(1+\alpha)} P^{-\alpha/(1+\alpha)} \qquad (26)$$

Substituting Eq.(22) into τ_{E0} of Eq.(26), the dependencies of energy confinement time can be derived:

$$\tau_E \propto n^{(\alpha+\beta)/(1+\alpha)} P^{-\alpha/(1+\alpha)} B^{a_2/(1+\alpha)} \times L^{(3\alpha+a_3)/(1+\alpha)} q^{-a_4/(1+\alpha)} . \qquad (27)$$

The international stellarator scaling law (ISSL-95) [17] is used as a reference empirical formula :

$$\tau_E^{ISSL} \propto n^{0.51} P^{-0.59} B^{0.83} L^{2.86} q^{-0.4} . \qquad (28)$$

Comparing Eqs.(27) and (28), the empirical scaling law (28) is interpreted as the confinement time with indices

$$\alpha \simeq 1.44 , \qquad (29\text{-}1)$$

$$\beta \simeq -0.2 , \qquad (29\text{-}2)$$

$$a_2 \simeq 2.03 , \qquad (29\text{-}3)$$

$$a_3 = 2.66 \ , \qquad (29\text{-}4)$$

and

$$a_4 = 0.976 \qquad (29\text{-}5)$$

The values of these coefficients are substituted into the power indices for the critical density in Eqs.(24-1)-(24-4). The power indices (c_1, c_2, c_3) are shown as a function of γ in Fig.4. One sees that, in a wide range of the index γ, the power index c_1 is approximately constant as

$$c_1 \sim \frac{1}{2} \ . \qquad (30)$$

On the other hand, the indices to the magnetic field and to the system size depend on the value of γ. In the limit of $\gamma = 0$, indices are given as

$$(c_1, c_2, c_3, c_4) = (0.5, 0, 1.5, 0) \ , \qquad (31)$$

i.e., $n_c \propto \sqrt{P/V}$, which corresponds to the simple estimate in which power dependence of L_z was neglected [1]. In a more realistic regime,

$$\gamma \sim 2 \qquad (32)$$

the indices are, very roughly speaking, given in the range of

$$(c_1, c_2, c_3, c_4) \sim \left(\frac{1}{2}, \frac{1}{2}, 1, \frac{1}{4}\right) \qquad (33)$$

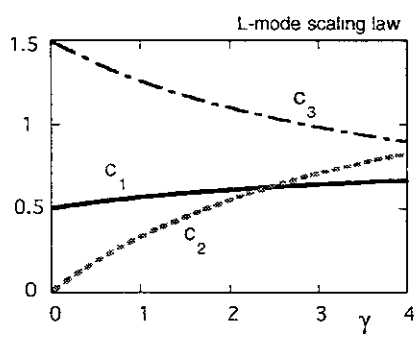

Fig.4 Power index as a function of the gradient of radiation coefficient $\gamma = -\partial \ell n(L_Z) / \partial \ell n(T)$. Empirical scaling law, ISSL-95, is used for the model of energy transport.

2.5.2 Deductive model of transport

Analysis is also performed for other transport models in which the transport coefficient is obtained by a deductive theory. We chose an example for the case of current-diffusive interchange mode turbulence [18]. This model has been shown to have considerable success in explaining the L-mode confinement. (The theory has also been extended to explain the H-mode, by introducing the effect of the radial electric field.) The formula of confinement time was deduced as

$$\tau_E \propto B^2 L^3 q^{-1} n^0 T^{-1.5} \ . \qquad (34)$$

The indices $(\alpha, \beta, a_2, a_3, a_4)$ are given as

$$(\alpha, \beta, a_2, a_3, a_4) = (1.5, 0, 2, 3.1) \qquad (35)$$

The indices for the density limit are then expressed as

$$c_1 = \frac{2.5 + \gamma}{5 + \gamma} \ , \qquad (36\text{-}1)$$

$$c_2 = \frac{2\gamma}{5+\gamma}, \qquad (36\text{-}2)$$

$$c_3 = \frac{7.5}{5+\gamma}, \qquad (36\text{-}3)$$

$$c_4 = \frac{\gamma}{5+\gamma} \qquad (36\text{-}4)$$

Figure 5 illustrates the dependence of coefficients on the parameter γ. Similar results are obtained in comparison with the case of the empirical form of transport loss.

2.6 Dependence of density limit

By considering the parameter dependence of the energy confinement time, the dependence of the critical density is deduced. A similar conclusion for the density limit is obtained when one employs either an empirical form of the energy confinement or a theoretical form of turbulent transport that is based on the current-diffusive interchange mode turbulence. This analysis shows that the relation $c_1 \sim 0.5$ holds independent of the shape of the radiation curve $\gamma = -d\,\ell n(L_Z)/d\,\ell n(T)$, so long as the impurity ratio n_I/n_e remains unaltered. The dependence of the transport loss on the magnetic field introduces the influence of the magnetic field on the critical density. The dependence of the confinement time on the plasma size affects additionally the dependence of critical density on the system size. The scaling dependence of the density limit is also influenced by the coefficient γ. The approximate estimation Eq.(33), $(c_1, c_2, c_3, c_4) \sim \left(\frac{1}{2}, \frac{1}{2}, 1, \frac{1}{4}\right)$, corresponds to an approximate form

$$n_c \sim P^{1/2} B^{1/2} V^{-1/3} q^{-1/4}. \qquad (37)$$

This result is compared to the experimental observation [2, 8]

$$n_c \propto \sqrt{PB/V}$$

The dependence on the heating power and magnetic field is close to the observation; Dependence on the plasma size becomes weaker than $n_c \propto V^{-1/2}$.

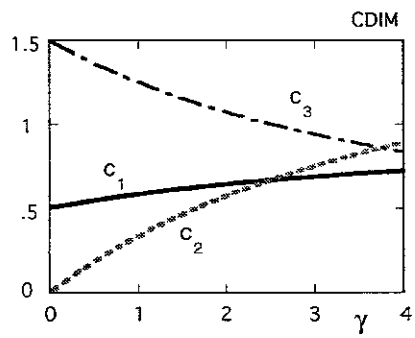

Fig.5 Power index as a function of the gradient of radiation coefficient $\gamma = -\partial\,\ell n(L_Z)/\partial\,\ell n(T)$. Transport model is based on current-diffusive interchange mode.

3. Dynamics at the Density Limit

3.1 Dynamical models

On the curve of Fig.2, the stationary solution is possible. When only the temperature is considered to evolve and other parameters are fixed, the direction of arrow in Fig.2 indicates the evolution of temperature. In the region where the transport dominates, (i.e., the right part of the curve), the stationary solution is stable. However, in the region where the radiation loss dominates, the stationary solution is unstable. A small deviation from the stationary curve causes further deviation of temperature from the curve.

The dynamical evolution is discussed in this chapter. When the density becomes higher than n_c, the stationary solution is lost, and the temperature starts to change. The other parameters might change as well. New type of dynamics could occur by the combination of the variation of other parameters.

The radiation loss is dependent on the plasma temperature, electron density and the impurity density. The transport loss of energy is also influenced by these parameters as well as by the radial electric field structure. The dynamical model of temperature collapse at the density limit consists of the particle balance equation,

$$\frac{d}{dt} n = -\frac{1}{\tau_p} n + S_p \qquad (38)$$

the equation of the momentum or the radial electric field

$$\frac{d}{dt} E_r = -\frac{1}{\tau_\phi} E_r - \hat{J}_r \qquad (39)$$

equation for temperature

$$\frac{d}{dt} T = -\frac{1}{\tau_E} T - \frac{P_{rad}}{3nV} + \frac{P_{abs}}{3nV} \qquad (40)$$

(where convective energy loss is included in $1/\tau_E$), and the particle balance equation for impurity,

$$\frac{d}{dt} n_I = -\frac{1}{\tau_I} n_I + S_I \,. \qquad (41)$$

Source terms are shown by S_p, $\hat{J}_r$, P_{abs} and S_I, and loss times are expressed as τ_p, τ_ϕ, τ_E, and τ_I.

In plasmas which are confined in toroidal helical plasmas, source terms as well as loss times are dependent on the plasma parameters as well as on the electric field. Nonlinear dependencies in these terms have been shown to cause self-sustained oscillations [19]. For instance, the dependence of τ_p (or τ_E) on the electric field and nonlinearity in $\hat{J}_r$ causes the limit cycle oscillation [20], which is attributed to the dithering ELMs [21]. This coupling has also been discussed [22] to understand the electric pulsation which was found in CHS device [23]. The influence of the radial electric field on P_{abs} [24], together with the dependence of electric field on temperature induces a thermo-electric oscillation [25]. Coupling between the transport coefficient and plasma profiles drives the nonlinear oscillation of confinement time [26]. The influence of temperature on the source of impurities was pointed out to cause oscillations being coupled with the nonlinearity in P_{rad} [27].

3.2 Reduction of Variables

Thus numerous types of self-generated oscillations in the system of dynamical equations are possible. A complete description of possible self-generated oscillations is not in the scope of this article. However, we intend to elucidate a new type of oscillation, by using a simplified dynamical model based on the method of reduction of variables. In the density limit oscillation of the W7-AS experiment [8], it was reported that (i) the relative ratio n_I/n_e changes little compared to the large amplitude oscillations of temperature or radiation loss and that (ii) hysteresis of loss in the energy transport, if it exists, is much smaller than that in the radiation loss. Based

on these observations, we employ the assumptions, as a first step of the analysis, that (i) n_I/n_e is constant in time and that (ii) τ_E is a single valued function (i.e., no hysteresis in it). Instead of solving Eq.(41), simplification (i) is applied. The next reduction of variable is the electric field. The radial electric field is self-sustained in helical plasmas due to the temperature gradient [28], and is subject to bifurcation, in principle, at a critical temperature [18, 28, 29]. Even though there is a possibility of a bifurcation in transport due to the bifurcation of radial electric field, in this article we do not consider such a mechanism and do not solve the dynamics of radial electric field Eq.(39). The inclusion of the radial electric field bifurcation is left for future work.

Based on these simplifying assumptions, we solve the coupled system of Eqs.(38) and (40). The sudden loss of density, which results from the radiation instability, is predicted to occur. When the radiation instability collapse continues and the temperature becomes lower than the critical value, the symmetry-breaking perturbations of temperature and potential on the magnetic surface become unstable. By the growth of these perturbations, the rapid loss takes place. The details are discussed in the Appendix. The critical condition for this instability is given in terms of the density and temperature as :

$$Tn^{-\gamma} \le \zeta \equiv \left(\frac{q^2 R^2}{3\chi_0} \frac{n_I}{n_e} \xi \right)^{1/(\gamma+3.5)}, \qquad y = \frac{2}{\gamma+3.5} \tag{42}$$

When this instability occurs, the rapid plasma loss happens as

$$\frac{d}{dt} n = -\frac{1}{\tau_M} n \tag{43}$$

where the right hand side represents the loss induced by this instability. An estimate of the loss rate of plasma density can be made as (see Appendix for the derivation)

$$\frac{1}{\tau_M} \sim \frac{s+\gamma}{C_a \tau_{rad}} \left(1 - \left(\frac{Tn^{-\gamma}}{\zeta} \right)^{\gamma+3.5} \right) \tag{44}$$

where s denotes the response of density to the inhomogeneous temperature perturbation, the coefficient $k_\perp^2 a^2 \sim C_a$ which is of the order unity, and

$$\frac{1}{\tau_{rad}} \equiv \frac{1}{3} \left(\frac{n_I}{n_e} \right) \xi n T_0^{-\gamma-1} \tag{45}$$

A minimal model, which is relevant to the study of density limit oscillation dynamics in W7-AS, is constructed from Eqs.(40), (43) and (44).

The prediction from Eqs.(43) and (44) is compared with the measurements. (See Fig.6.) It is observed that the rate of density change, $n^{-1}dn/dt$, is fitted to a single valued function during the oscillation of energy in W7-AS. The loss rate $n^{-1}dn/dt$ changes its sign dramatically when the temperature-to-density ratio becomes lower than some critical value.

3.3 Model of density limit oscillation

A minimal model for the density limit oscillation is constructed by Eq.(40) together with Eq.(43) and (44). The flow

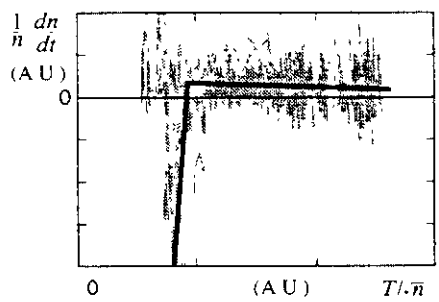

Fig.6 Observation on W7-AS stellarator. During the several cycles of density limit oscillation, the rate of density change is correlated with the temperature. Rate of density change, $n^{-1}dn/dt$, is fitted to a single valued function of $T/\sqrt{n}$ during the limit cycle oscillation. Strong loss of density sets in if temperature becomes very low. Thick solid line is an eye guide. (Units are arbitrary)

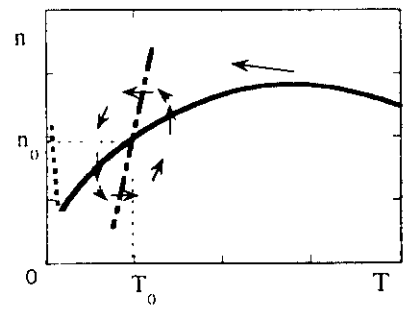

Fig.7 Flow diagram. Solid lines and thick dot-dashed lines represent the stationary solution of Eqs.(43) and (44), respectively. The arrow shows the temporal change in n and T, $\left(dT/dt, dn/dt\right)$.

diagram is shown schematically on Fig.7. The stationary solution of Eq.(40) is shown by the solid line, and that for Eq.(43), $1/\tau_M = 0$, is plotted by the thick dot-dashed line Their intersection represents the fixed point $\left(T_0, n_0\right)$. The temporal change in n and T, $\left(dT/dt, dn/dt\right)$, is shown by the arrow for various points on the $\left(T, n\right)$ plane. Noting the change of signs near by the fixed point, the flow pattern is found to encircle the fixed point, in the vicinity of the fixed point.

We study the dynamic of variables near the fixed point $\left(T_0, n_0\right)$, where $\left(T_0, n_0\right)$ satisfy both of the stationary equations, i.e., the limit of $dl/dt \to 0$ of (40) and (43);

$$\left(\frac{P_{abs}}{3\,n_0\,V} - \frac{1}{\tau_E\left(T_0, n_0\right)}\,T_0\right) - \frac{P_{rad}\left(T_0, n_0\right)}{3\,n_0\,V} = 0 \qquad (46)$$

and

$$T_0 n_0^{\gamma} = \zeta \qquad (47)$$

The case of strong radiation, $P_{rad} >> W/\tau_E$ at $\left(T_0, n_0\right)$, is considered. Combining Eq (5) with Eq.(40), one has

$$\frac{d}{dt}\,T = \frac{P_{abs}}{3\,n\,V} - \frac{1}{3}\left(\frac{n_I}{n}\right)\xi\,T^{-\gamma}\,n \qquad (48)$$

Noting that $\left(T_0, n_0\right)$ satisfy the equation of stationary state, $\frac{P_{abs}}{n_0 V} - \left(\frac{n_I}{n}\right)\xi\,T_0^{-\gamma}\,n_0 = 0$, Eq.(48) is rewritten as

$$\frac{d}{dt}\,T = \frac{P_{abs}}{3\,n_0\,V}\left(\frac{n_0}{n} - 1\right) + \frac{1}{3}\left(\frac{n_I}{n}\right)\xi\left(T_0^{-\gamma}\,n_0 - T^{-\gamma}\,n\right). \qquad (49)$$

By using the time rate of change τ_{rad} defined in Eq.(45), Eq.(49) can be rewritten as

$$\frac{d}{dt}\,\frac{T}{T_0} = \frac{1}{\tau_{rad}}\left(\frac{n_0}{n} - \left(\frac{T_0}{T}\right)^{\gamma}\frac{n}{n_0}\right) \qquad (50)$$

The stability of the trajectory near the fixed point is investigated. We put

$$T = T_0\left(1 + \delta T\right) \qquad (51\text{-}1)$$

and

$$n = n_0\left(1 + \delta n\right) . \qquad (51\text{-}2)$$

In the vicinity of $\left(T_0, n_0\right)$, the Taylor expansions of Eqs.(43), (44) and (50) are made. By use of this expansion, Eq.(43) with Eq.(44) and Eq.(50) are rewritten as, respectively,

$$\frac{d}{dt}\delta n = -\frac{y}{\tau}\delta n + \frac{1}{\tau}\delta T \qquad (52)$$

and

$$\frac{d}{dt}\delta T = -\frac{1}{\tau_1}\delta n + \frac{1}{\tau_2}\delta T . \qquad (53)$$

where the time constants τ, τ_1 and τ_2 are expressed as

$$\frac{1}{\tau} = \frac{\left(s+\gamma\right)\left(\gamma+3.5\right)}{C_a}\frac{1}{\tau_{rad}} \qquad (54\text{-}1)$$

$$\frac{1}{\tau_1} = \frac{2}{\tau_{rad}} , \qquad (54\text{-}2)$$

$$\frac{1}{\tau_2} = \frac{\gamma}{\tau_{rad}} . \qquad (54\text{-}3)$$

Equations (52) and (53) are solved assuming that the temporal dependence is written as

$$\left(\delta n, \delta T\right) \propto e^{\lambda t} \qquad (55)$$

The eigenvalue λ is obtained as

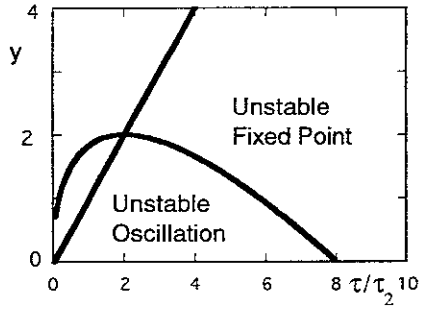

Fig.8 Parameter region that allows an unstable oscillatory solution. Case of $\tau_2/\tau_1 = 2$ is shown.

$$\lambda = \frac{\frac{1}{\tau_2} - \frac{y}{\tau} \pm \sqrt{\left(\frac{1}{\tau_2} + \frac{y}{\tau}\right)^2 - \frac{4}{\tau_1\tau}}}{2} . \qquad (56)$$

An oscillatory solution exists if the condition

$$\frac{4}{\tau_1\tau} > \left(\frac{1}{\tau_2} + \frac{y}{\tau}\right)^2 \qquad (57)$$

holds. An unstable oscillation exists if

$$\frac{1}{\tau_2} > \frac{y}{\tau} \qquad (58)$$

is satisfied together with Eq.(57).

The limit cycle oscillation is possible in the region that is denoted as 'unstable oscillation' in Fig.8. This diagram presents the condition for the density limit oscillation. A small value of τ/τ_2 is necessary. This means that the abrupt reduction of density at $T n^{-y} \sim \zeta$ is the key for the oscillation. Conditions Eqs.(57) and (58) for unstable oscillation are rewritten, in terms of the

parameter γ that characterizes the radiation rate, as

$$\frac{8(s+\gamma)(\gamma+3.5)}{C_a} > \left(\gamma+\frac{2(s+\gamma)}{C_a}\right)^2 \quad (57')$$

$$\gamma > \frac{2(s+\gamma)}{C_a} \quad (58')$$

In order to satisfy the instability condition, Eq (58'), $C_a > 2$ is the necessary condition. If it is satisfied, Eqs.(57') and (58') is rewritten as

$$\frac{2s}{C_a-2} < \gamma < \frac{2C_a(7+s)-4s}{(C_a-2)^2} + \frac{2\sqrt{\left(C_a(7+s)-2s\right)^2-(C_a-2)^2(s^2-7sC_a)}}{(C_a-2)^2} \quad (59)$$

For intermediate values of γ that satisfy Eq.(59), an unstable oscillation near the fixed point is predicted. The actual range of γ for the limit cycle solution depends on the parameters (s, C_a), which appears in the response of plasma to the inhomogeneous perturbation of density. Although quantitative values of the parameters (s, C_a) are determined by a detailed analysis of transport models , it is beyond the scope of this article to carry this out. Only a qualitative conclusion is possible here. The parameter γ depends on the species of the impurity and range of operation temperature [10]. The condition (59) limits the impurity species that can cause oscillation.

If γ is very large, i.e., the radiation cooling curve $L_Z(T)$ is very steep, so as to exceed the right hand side of Eq (59), then the fixed point is unstable but not oscillatory. In such cases, the trajectory continuously deviates from the fixed point and might approach to the another fixed point. Usually, the other fixed point exists in a much lower branch of the radiation cooling curve (e.g., dotted line in Fig.2) The density limit collapse occurs, without the recovery of high temperature plasma. The rate of density decay dictates whether the oscillation takes place or radiation collapse continues when the density exceeds the critical density.

In the case of small values of γ, Eq.(58') is not satisfied, that is, the fixed point (T_0, n_0) in Fig.7 is a stable fixed point. The stability of this fixed point means that the steady state is realized in the region where the conditions $d\{L_Z(T)\}/dT < 0$ and $\partial P_{in}/\partial T < 0$ are satisfied. This is a new type of steady state which is originated from the rapid loss of density with the condition given by Eq.(47).

4. Summary and Discussion

The physics of the density limit phenomena in toroidal helical plasmas based on an analytic point model of toroidal plasmas was discussed. The combination of the transport and radiation loss of energy was analyzed. Firstly, the scaling law of the density limit was derived as a static relation. The dependence of the critical density on the heating power, magnetic field, plasma size and safety factor is explained. Next, the dynamical evolution of the plasma energy and radiation loss is discussed. Employing a simple model of density evolution a limit cycle oscillation is predicted, when a sudden reduction of density

occurs due to the symmetry-breaking radiation instability caused by reaching a critically low temperature. The condition that divides the limit cycle oscillation and the complete radiation collapse was derived. This model seems to explain the density limit oscillation that has been observed on W7-AS [8]. Further comparative studies of the "breathing phenomena" in LHD [6,7] and the density limit oscillation in CHS [16] are necessary to determine whether or not this model also applies.

The dependence of the density limit like $n_c \sim P^{1/2} B^{1/2} V^{-1/3} q^{-1/4}$ is obtained in the range of $\gamma = -d\ell n(L_Z)/d\ell n(T) \sim 2$. This form is close to what has been reported from empirical studies [2. 8] but the dependence on the plasma size becomes weaker than $n_c \propto V^{-1/2}$. Regression analysis on experimental data has been performed until now on the variables B and P/V . In future studies, the independent fitting of the critical density to the heating power and plasma volume is necessary. In addition, the limiting density depends on the ratio of impurity density to the electron density. The heating method could have a strong impact on the source of impurities and in turn change the parameter $\xi n_i/n_e$. The density limit could therefore depend on the heating method. This point must be clarified in future experiments.

The impact of indices (c_1, c_2, c_3, c_4) for the future prospects of the achievable fusion triplet value

$$n\tau_E T = \frac{P}{V}\tau_E^2 \qquad (60)$$

is discussed assuming that the parameter $\xi n_i/n_e$ is constant. Substitution of Eq.(27) provides the relation

$$n\tau_E T \propto n^{2(\alpha+\beta)/(1+\alpha)} P^{(1-\alpha)/(1+\alpha)} B^{2a_2/(1+\alpha)} \times L^{(3\alpha-3+2a_3)/(1+\alpha)} q^{-2a_4/(1+\alpha)} \qquad (61)$$

The density is bound by the density limit, $n \le n_c$. The upper bound of n provides the upper bound of the fusion triplet

$$n\tau_E T \le (n\tau_E T)_{\max} \qquad (62)$$

The parameter dependence of $(n\tau_E T)_{\max}$ is derived by substituting the dependencies of the density limit Eqs.(24-1)-(24-4) into Eq.(61), and one has the scaling relation

$$(n\tau_E T)_{\max} \propto P^{d_1} B^{d_2} L^{d_3} q^{-d_4} \qquad (63)$$

with

$$d_1 = \frac{(1+\beta)(2+\gamma)}{2+2\alpha+(1-\beta)\gamma} \qquad (64\text{-}1)$$

$$d_2 = \frac{2a_2(2+\gamma)}{2+2\alpha+(1-\beta)\gamma} \qquad (64\text{-}2)$$

$$d_3 = \frac{\{2a_3 - 3(1+\beta)\}(2+\gamma)}{2+2\alpha+(1-\beta)\gamma} \qquad (64\text{-}3)$$

$$d_4 = \frac{2a_4(2+\gamma)}{2+2\alpha+(1-\beta)\gamma} \qquad (64\text{-}4)$$

Figure 9 describes the dependencies of indices (d_1, d_2, d_3) as a function of γ . In the range of $\gamma \simeq 2$, the estimate $(d_1, d_2, d_3, d_4) \simeq (0.44, 2.2, 1.6, 1.1)$ is given

for the empirical form of the L-mode confinement law.

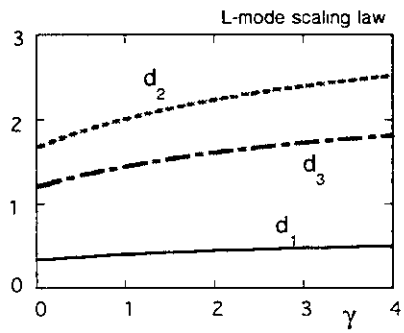

Fig.9 Dependencies of indices (d_1, d_2, d_3) as a function of γ .

This dependence of fusion triplet describes how the magnetic field, system size and heating power are effective in improving the fusion triplet number. The knowledge of the density limit is essential for the future prospects of helical devices for fusion research. For instance, the predicted critical density is influenced by the difference between the dependence of $n_c \propto V^{-1/3}$ in this article and $n_c \propto V^{-1/2}$ in previous empirical fits. (Note that the dependence on volume has not been independently fitted in previous empirical scaling studies.) The weaker dependence of density limit on plasma volume leads to a better extrapolated value. A systematic investigation of experimental data from a number of fusion devices with the presented theoretical ideas as a reference point would be valuable.

Acknowledgements:

Two of the authors (KI and SII) acknowledge hospitality of Alexander von Humboldt Stiftung, Max-Planck-Institut fur Plasmaphysik, and Prof. F. Wagner, which is essential for this research. Part of this study has been performed when one of the authors (LG) was visiting National Institute for Fusion Science by the Grant-in-Aid for International Collaboration of Ministry of Education, Japan. This work is also partly supported by the Grant-in-Aid for Scientific Research of Ministry of Education, Japan.

Appendix: Density Decay at Low Density

Temperature and potential perturbations can grow due to a radiation instability. The variation of temperature on the magnetic surface is introduced as

$$T(r,\theta) = T_0(r) + \tilde{T}(r,\theta) \qquad \text{(A1)}$$

The poloidal-angle-dependent component of the energy balance equation is given as

$$\frac{\partial}{\partial t}\tilde{T} = \delta\left\{-\frac{1}{3}(n_I/n_e)\xi n T^{-\gamma} + \nabla_{\parallel}\chi_{\parallel}\nabla_{\parallel}T + \nabla_{\perp}\chi_{\perp}\nabla_{\perp}T\right\} \qquad \text{(A2)}$$

where the symbol $\delta\{X\}$ implies the poloidally-dependent part of the quantity X . The inhomogeneity of the heating is neglected, as it is the source of possible variation on a magnetic surface. This is done in order to illustrate the impact of spontaneous symmetry breaking. The relative variation of the radiation rate is parameterized by the coefficient s as

$$\left(\frac{n_I}{n_e}\right)\xi n = \left[\left(\frac{n_I}{n_e}\right)\xi n\right]_0\left(1 - s\frac{\tilde{T}}{T_0}\right) \qquad \text{(A3)}$$

A positive value of s includes the process that the electron density is higher in the region of lower electron temperature. Such a density variation arises from the potential variation. Noting the relation $\nabla_{\parallel}^2 T = -q^{-2}R^{-2}\tilde{T}$, Eq.(A3) is rewritten as

$$\frac{\partial}{\partial t}\tilde{T} = \gamma_M \tilde{T} \qquad \text{(A4)}$$

where

$$\gamma_M \equiv \frac{1}{3}(\gamma + s)\left(\frac{n_I}{n_e}\right)\xi n T_0^{-\gamma-1} - \frac{\chi_{\parallel}}{q^2R^2} \qquad \text{(A5)}$$

In calculating the growth rate γ_M, the perpendicular diffusion term is neglected, because the perpendicular loss rate is smaller than the radiation loss rate after the radiation collapse takes place. Noticing the dependence of the parallel conductivity on the temperature,

$$\chi_{\parallel} = \chi_0 n^{-1} T^{2.5} \qquad \text{(A6)}$$

the instability condition $\gamma_M > 0$ can be rewritten as

$$Tn^{-y} \le \zeta \equiv \left(\frac{q^2R^2}{3\chi_0}\frac{n_I}{n_e}\xi\right)^{1/(\gamma+3.5)}, \quad y = \frac{2}{\gamma+3.5} \qquad \text{(A7)}$$

When this instability occurs, the rapid plasma loss occurs. We use a simple model of

$$\frac{d}{dt}n = -\frac{1}{\tau_M}n \qquad \text{(A8)}$$

where the right hand side represents the loss induced by this instability. An estimate of the loss rate of plasma density can be made, by use of the growth rate γ_M and the perpendicular wave number $k_{\perp}$ of the instability Eq.(A4), as

$$\frac{1}{\tau_M} \simeq \frac{\gamma_M}{k_{\perp}^2}\frac{1}{a^2} \qquad \text{(A9)}$$

With the order estimate of

$$k_{\perp}^2 a^2 \sim C_a$$

which is of the order unity, one obtains

$$\frac{1}{\tau_M} \sim \frac{s+\gamma}{C_a \tau_{rad}}\left(1 - \left(\frac{Tn^{-y}}{\zeta}\right)^{\gamma+3.5}\right) \qquad \text{(A10)}$$

where

$$\frac{1}{\tau_{rad}} \equiv \frac{1}{3}\left(\frac{n_I}{n_e}\right)\xi n T_0^{-\gamma-1} \qquad \text{(A11)}$$

Rapid plasma loss is predicted to occur at low temperature, Eq.(A7).

References

[1] Itoh K and Itoh S-I 1988 *J. Phys. Soc. Jpn.* **57** 1269.
[2] Sudo S, Takeiri Y. Zushi H, et al. 1990 *Nucl. Fusion* **30**, 11.
[3] Wagner F et al. 1994 *Plasma Phys. Controlled Fusion* **36**, A61.
[4] Giannone L et al. 1999 *Journal of Nucl. Materials* **266-269**, 501.
[5] Fujiwara M 1999 *Plasma Phys. Controlled Fusion* **41** in press
[6] Takeiri Y, Noda N, Kaneko O, et al. 1999 26th European Conference on Controlled Fusion and Plasma Physics (Maastricht) 23J, 1365.
[7] Peterson B J, et al. 1999 26th European Conference on Controlled Fusion and Plasma Physics (Maastricht)P3.104
[8] Giannone L, et al. 1999 'Physics of the density limit in the W7-AS Stellarator' (IPP-Report III/252, 1999) submitted to *Plasma Phys. Controlled Fusion.*
[9] Grigull P. Hirsch M, McCormick K, et al. 1999 26th European Conference on Controlled Fusion and Plasma Physics (Maastricht) 23J, 1473.

[10] Post D, Jensen R, Tarter C, Grasberger W, and Lokke W 1977 *Atomic Data and Nuclear Tables* **20** 397.
[11] Lipschultz B et al. 1984 *Nucl. Fusion* **24** 977.
Stringer T E 1985 *Controlled Fusion and Plasma Physics*, Proceedings of the 12th EPS Conference, (Budapest) Vol.9F, Part I, p 86.
Wesson J A et al. 1985, *ibid.* 147.
Neuhauser J, Schneider W Z, Wunderlich R 1986 *Nucl Fusion* **26** 1679
Drake J F 1987 *Phys. Fluids* **30** 2429
Ohyabu N 1979 *Nucl. Fusion* **19** 1491.
[12] Murakami M et al. 1976 *Nucl. Fusion* **16** 347
Fielding S J et al 1977 *Nucl Fusion* **17** 1382
Greenwald M, Terry J, Wolfe S, et al. 1988 *Nucl. Fusion* **28** 2199.
[13] Hawryluk R J, et al. 1979 *Nucl. Fusion* **19** 1307
[14] Kaneko H, Kondo K, Motojima O, et al. 1987 *Nucl Fusion* **27**, 1075.
[15] Burhenn R et al. 1997 24th European Conference on Controlled Fusion and Plasma Physics (Berchtesgaden) IV, 1659
[16] Okamura S 1999 private communications
[17] Stroth U et al. 1996 *Nucl. Fusion* **36** 1063.
[18] Itoh K, Itoh S-I and Fukuyama A 1992 *Phys. Rev. Lett.* **69** 1050
[19] Itoh K, Itoh S-I, Fukuyama A; *Transport and Structural Formation in Plasmas* (IoP, Bristol, England, 1999).
[20] Itoh S-I, Itoh K, Fukayama A, Miura Y and JFT-2M Group 1991 *Phys. Rev. Lett.* **67** 2485
Itoh S-I, et al 1991 Research Report NIFS-96.
[21] ASDEX Team 1989 *Nucl Fusion* **29** 1959
[22] Itoh K, et al. 1999 26th European Conference on Controlled Fusion and Plasma Physics (Maastricht) 23J, P3.095
[23] Fujisawa A et al. 1998 *Phys. Rev. Lett.* **81** 2256
[24] Sanuki H, Itoh K and Itoh S-I 1993 *J. Phys. Soc. Jpn.* **62** 123
[25] Itoh K et al. 1994 *Phys. Plasmas* **1** 796
[26] Fukuyama A et al. 1995 *Nucl. Fusion* **35** 1669.
[27] Tokar 1999 private communications
[28] Kovrizhnykh L M 1984 *Nucl. Fusion* **24** 435.
[29] Sanuki H et al. 2000 J. Phys. Soc. Jpn. 69 No.2 in press.

Recent Issues of NIFS Series

NIFS-563 Y Todo and T. Sato,
Kinetic-Magnetohydrodynamic Simulation Study of Fast Ions and Toroidal Alfvén Eigenmodes; Oct 1998
(IAEA-CN-69/THP2/22)

NIFS-564 T Watari, T Shimozuma, Y. Takeiri, R Kumazawa, T Mutoh, M Sato, O Kaneko, K. Ohkubo, S. Kubo, H Idei, Y Oka, M Osakabe, T Seki, K Tsumori, Y. Yoshimura, R. Akiyama, T Kawamoto, S. Kobayashi, F Shimpo, Y Takita, E. Asano, S Itoh, G Nomura, T Ido, M Hamabe, M Fujiwara, A Iiyoshi, S. Morimoto, T Bigelow and Y.P Zhao.
Steady State Heating Technology Development for LHD, Oct. 1998
(IAEA-CN-69/FTP/21)

NIFS-565 A Sagara, K.Y Watanabe, K Yamazaki, O Motojima, M. Fujiwara, O Mitarai, S Imagawa, H Yamanishi, H Chikaraishi, A Kohyama, H. Matsui, T. Muroga, T Noda, N. Ohyabu, T. Satow, A.A. Shishkin, S. Tanaka, T. Terai and T. Uda,
LHD-Type Compact Helical Reactors, Oct 1998
(IAEA-CN-69/FTP/03(R)

NIFS-566 N. Nakajima, J. Chen, K Ichiguchi and M. Okamoto,
Global Mode Analysis of Ideal MHD Modes in L=2 Heliotron/Torsatron Systems; Oct 1998
(IAEA-CN-69/THP1/08)

NIFS-567 K Ida, M. Osakabe, K Tanaka, T Minami, S. Nishimura, S. Okamura, A Fujisawa, Y. Yoshimura, S. Kubo, R. Akiyama, D.S Darrow, H. Idei, H Iguchi, M. Isobe, S. Kado, T. Kondo, S. Lee, K Matsuoka, S. Morita, I. Nomura, S. Ohdachi, M Sasao, A Shimizu, K Tumori, S. Takayama, M. Takechi, S. Takagi, C Takahashi, K Toi and T Watari,
Transition from L Mode to High Ion Temperature Mode in CHS Heliotron/Torsatron Plasmas, Oct 1998
(IAEA-CN-69/EX2/2)

NIFS-568 S. Okamura, K Matsuoka, R. Akiyama, D.S Darrow, A Ejiri, A. Fujisawa, M Fujiwara, M. Goto, K Ida H. Idei, H Iguchi, N Inoue, M Isobe, K Itoh, S. Kado, K Khlopenkov, T. Kondo, S. Kubo, A Lazaros, S. Lee, G. Matsunaga, T Minami, S. Morita, S Murakami, N Nakajima, N. Nikai, S. Nishimura, I Nomura, S. Ohdachi, K Ohkuni, M Osakabe, R. Pavlichenko, B. Peterson, R Sakamoto, H Sanuki, M. Sasao, A Shimizu, Y Shirai, S. Sudo, S. Takagi, C Takahashi, S. Takayama, M Takechi, K Tanaka, K Toi, K Yamazaki, Y Yoshimura and T Watari,
Confinement Physics Study in a Small Low-Aspect-Ratio Helical Device CHS; Oct 1998
(IAEA-CN-69/OV4/5)

NIFS-569 M.M. Skoric, T. Sato, A. Maluckov, M.S. Jovanovic,
Micro- and Macro-scale Self-organization in a Dissipative Plasma, Oct 1998

NIFS-570 T. Hayashi, N. Mizuguchi, T-H Watanabe, T. Sato and the Complexity Simulation Group,
Nonlinear Simulations of Internal Reconnection Event in Spherical Tokamak; Oct. 1998
(IAEA-CN-69/TH3/3)

NIFS-571 A Iiyoshi, A. Komori, A Ejiri, M. Emoto, H Funaba, M. Goto, K Ida, H Idei, S. Inagaki, S. Kado, O Kaneko, K Kawahata, S. Kubo, R Kumazawa, S. Masuzaki, T Minami, J Miyazawa, T. Morisaki, S Morita, S. Murakami, S Muto, T. Muto, Y Nagayama, Y Nakamura, H. Nakanishi, K Narihara, K Nishimura, N Noda, T Kobuchi, S Ohdachi, N. Ohyabu, Y Oka, M Osakabe, T. Ozaki, B.J. Peterson, A Sagara, S Sakakibara, R Sakamoto, H Sasao, M. Sasao, K Sato, M Sato, T Seki, T Shimozuma, M. Shoji, H Suzuki, Y Takeiri, K Tanaka, K Toi, T Tokuzawa, K Tsumori, I. Yamada, H Yamada, S Yamaguchi, M Yokoyama, K.Y.Watanabe, T Watari, R Akiyama, H. Chikaraishi, K Haba, S. Hamaguchi, S. Iima, S. Imagawa, N Inoue, K Iwamoto, S. Kitagawa, Y Kubota, J. Kodaira, R. Maekawa, T Mito. T. Nagasaka, A Nishimura, Y. Takita, C. Takahashi, K Takahata, K Yamauchi, H. Tamura, T. Tsuzuki, S. Yamada, N. Yanagi, H Yonezu, Y. Hamada, K Matsuoka, K Murai, K Ohkubo, I. Ohtake, M Okamoto, S. Sato, T. Satow, S. Sudo, S Tanahashi, K Yamazaki, M. Fujiwara and O Motojima,
An Overview of the Large Helical Device Project; Oct 1998
(IAEA-CN-69/OV1/4)

NIFS-572 M Fujiwara, H. Yamada, A Ejiri, M Emoto, H Funaba, M. Goto, K Ida, H. Idei, S. Inagaki, S. Kado, O. Kaneko, K Kawahata, A Komori, S. Kubo, R. Kumazawa, S. Masuzaki, T Minami, J. Miyazawa, T. Morisaki, S. Morita, S. Murakami, S. Muto, T. Muto, Y. Nagayama, Y. Nakamura, H. Nakanishi, K. Narihara, K. Nishimura, N. Noda, T. Kobuchi, S. Ohdachi, N. Ohyabu, Y. Oka, M. Osakabe, T. Ozaki, B. J. Peterson, A. Sagara, S. Sakakibara, R Sakamoto, H. Sasao, M. Sasao, K Sato, M Sato, T. Seki, T Shimozuma, M Shoji, H. Sazuki, Y. Takeiri, K Tanaka, K Toi, T Tokuzawa, K Tsumori, I. Yamada, S. Yamaguchi, M Yokoyama, K.Y. Watanabe, T Watari, R. Akiyama, H. Chikaraishi, K Haba, S. Hamaguchi, M. Iima, S. Imagawa, N. Inoue, K Iwamoto, S. Kitagawa, Y. Kubota, J. Kodaira, R. Maekawa, T Mito, T. Nagasaka, A. Nishimura, Y. Takita, C. Takahashi, K Takahata, K Yamauchi, H. Tamura, T Tsuzuki, S. Yamada, N. Yanagi, H Yonezu, Y. Hamada, K Matsuoka, K Murai, K Ohkubo, I Ohtake, M. Okamoto, S. Sato, T Satow, S. Sudo, S. Tanahashi, K Yamazaki, O Motojima and A Iiyoshi,
Plasma Confinement Studies in LHD; Oct 1998
(IAEA-CN-69/EX2/3)

NIFS-573 O Motojima, K. Akaishi, H. Chikaraishi, H. Funaba, S. Hamaguchi, S. Imagawa, S. Inagaki, N. Inoue, A. Iwamoto, S. Kitagawa, A. Komori, Y. Kubota, R. Maekawa, S. Masuzaki, T Mito, J. Miyazawa, T Morisaki, T. Muroga, T. Nagasaka, Y Nakmura, A Nishimura, K Nishimura, N. Noda, N. Ohyabu, S. Sagara, S. Sakakibara, R. Sakamoto, S. Satoh, T Satow, M Shoji, H. Suzuki, K Takahata, H Tamura, K Watanabe, H Yamada, S Yamada, S. Yamaguchi, K Yamazaki, N. Yanagi, T Baba, H. Hayashi, M. Iima, T. Inoue, S. Kato, T Kato, T Kondo, S. Moriuchi, H. Ogawa, I Ohtake, K Ooba, H Sekiguchi, N. Suzuki, S. Takami, Y. Taniguchi, T Tsuzuki, N. Yamamoto, K Yasui, H Yonezu, M Fujiwara and A Iiyoshi,
Progress Summary of LHD Engineering Design and Construction; Oct 1998

(IAEA-CN-69/FT2/1)

NIFS-574 K. Toi, M. Takechi, S. Takagi, G. Matsunaga, M. Isobe, T. Kondo, M. Sasao, D.S. Darrow, K. Ohkuni, S. Ohdachi, R. Akiyama, A. Fujisawa, M. Gotoh, H. Idei, K. Ida, H. Iguchi, S. Kado, M. Kojima, S. Kubo, S. Lee, K. Matsuoka, T. Minami, S. Monta, N. Nikai, S. Nishimura, S. Okamura, M. Osakabe, A. Shimizu, Y. Shirai, C. Takahashi, K. Tanaka, T. Watari and Y. Yoshimura,
Global MHD Modes Excited by Energetic Ions in Heliotron/Torsatron Plasmas; Oct. 1998
(IAEA-CN-69/EXP1/19)

NIFS-575 Y. Hamada, A. Nishizawa, Y. Kawasumi, A. Fujisawa, M. Kojima, K. Narihara, K. Ida, A. Ejiri, S. Ohdachi, K. Kawahata, K. Toi, K. Sato, T. Seki, H. Iguchi, K. Adachi, S. Hidekuma, S. Hirokura, K. Iwasaki, T. Ido, R. Kumazawa, H. Kuramoto, T. Minami, L. Nomura, M. Sasao, K.N. Sato, T. Tsuzuki, I. Yamada and T. Watari,
Potential Turbulence in Tokamak Plasmas; Oct. 1998
(IAEA-CN-69/EXP2/14)

NIFS-576 S. Murakami, U. Gasparino, H. Idei, S. Kubo, H. Maassberg, N. Marushchenko, N. Nakajima, M. Romé and M. Okamoto,
5D Simulation Study of Suprathermal Electron Transport in Non-Axisymmetric Plasmas; Oct. 1998
(IAEA-CN-69/THP1/01)

NIFS-577 S. Fujiwara and T. Sato,
Molecular Dynamics Simulation of Structure Formation of Short Chain Molecules; Nov. 1998

NIFS-578 T. Yamagishi,
Eigenfunctions for Vlasov Equation in Multi-species Plasmas Nov. 1998

NIFS-579 M. Tanaka, A. Yu. Grosberg and T. Tanaka,
Molecular Dynamics of Strongly-Coupled Multichain Coulomb Polymers in Pure and Salt Aqueous Solutions; Nov. 1998

NIFS-580 J. Chen, N. Nakajima and M. Okamoto,
Global Mode Analysis of Ideal MHD Modes in a Heliotron/Torsatron System: I. Mercier-unstable Equilibria; Dec. 1998

NIFS-581 M. Tanaka, A. Yu. Grosberg and T. Tanaka,
Comparison of Multichain Coulomb Polymers in Isolated and Periodic Systems: Molecular Dynamics Study; Jan. 1999

NIFS-582 V.S. Chan and S. Murakami,
Self-Consistent Electric Field Effect on Electron Transport of ECH Plasmas; Feb. 1999

NIFS-583 M. Yokoyama, N. Nakajima, M. Okamoto, Y. Nakamura and M. Wakatani,
Roles of Bumpy Field on Collisionless Particle Confinement in Helical-Axis Heliotrons; Feb. 1999

NIFS-584 T.-H. Watanabe, T. Hayashi, T. Sato, M. Yamada and H. Ji,
Modeling of Magnetic Island Formation in Magnetic Reconnection Experiment; Feb. 1999

NIFS-585 R. Kumazawa, T. Mutoh, T. Seki, F. Shinpo, G. Nomura, T. Ido, T. Watari, Jean-Marie Noterdaeme and Yangping Zhao,
Liquid Stub Tuner for Ion Cyclotron Heating; Mar. 1999

NIFS-586 A. Sagara, M. Iima, S. Inagaki, N. Inoue, H. Suzuki, K. Tsuzuki, S. Masuzaki, J. Miyazawa, S. Morita, Y. Nakamura, N. Noda, B. Peterson, S. Sakakibara, T. Shimozuma, H. Yamada, K. Akaishi, H. Chikaraishi, H. Funaba, O. Kaneko, K. Kawahata, A. Komori, N. Ohyabu, O. Motojima, LHD Exp. Group 1, LHD Exp. Group 2,
Wall Conditioning at the Starting Phase of LHD; Mar. 1999

NIFS-587 T. Nakamura and T. Yabe,
Cubic Interpolated Propagation Scheme for Solving the Hyper-Dimensional Vlasov-Poisson Equation in Phase Space; Mar. 1999

NIFS-588 W.X. Wnag, N. Nakajima, S. Murakami and M. Okamoto,
An Accurate δf Method for Neoclassical Transport Calculation; Mar. 1999

NIFS-589 K. Kishida, K. Araki, S. Kishiba and K. Suzuki,
Local or Nonlocal? Orthonormal Divergence-free Wavelet Analysis of Nonlinear Interactions in Turbulence; Mar. 1999

NIFS-590 K. Araki, K. Suzuki, K. Kishida and S. Kishiba,
Multiresolution Approximation of the Vector Fields on T^3; Mar. 1999

NIFS-591 K. Yamazaki, H. Yamada, K.Y. Watanabe, K. Nishimura, S. Yamaguchi, H. Nakanishi, A. Komori, H. Suzuki, T. Mito, H. Chikaraishi, K. Murai, O. Motojima and the LHD Group,
Overview of the Large Helical Device (LHD) Control System and Its First Operation, Apr. 1999

NIFS-592 T. Takahashi and Y. Nakao,
Thermonuclear Reactivity of D-T Fusion Plasma with Spin-Polarized Fuel, Apr. 1999

NIFS-593 H. Sugama,
Damping of Toroidal Ion Temperature Gradient Modes, Apr. 1999

NIFS-594 Xiaodong Li,
Analysis of Crowbar Action of High Voltage DC Power Supply in the LHD ICRF System; Apr. 1999

NIFS-595 K. Nishimura, R. Horiuchi and T. Sato,
Drift-kink Instability Induced by Beam Ions in Field-reversed Configurations, Apr. 1999

NIFS-596 Y. Suzuki, T-H. Watanabe, T. Sato and T. Hayashi,
Three-dimensional Simulation Study of Compact Toroid Plasmoid Injection into Magnetized Plasmas; Apr. 1999

NIFS-597 H. Sanuki, K. Itoh, M. Yokoyama, A. Fujisawa, K. Ida, S. Toda, S.-I. Itoh, M. Yagi and A. Fukuyama,
Possibility of Internal Transport Barrier Formation and Electric Field Bifurcation in LHD Plasma, May 1999

NIFS-598 S. Nakazawa, N. Nakajima, M. Okamoto and N. Ohyabu,
One Dimensional Simulation on Stability of Detached Plasma in a Tokamak Divertor, June 1999

NIFS-599 S. Murakami, N. Nakajima, M. Okamoto and J. Nihrenberg,
Effect of Energetic Ion Loss on ICRF Heating Efficiency and Energy Confinement Time in Heliotrons; June 1999

NIFS-600 R. Horiuchi and T. Sato,
Three-Dimensional Particle Simulation of Plasma Instabilities and Collisionless Reconnection in a Current Sheet;; June 1999

NIFS-601 W. Wang, M. Okamoto, N. Nakajima and S. Murakami,
Collisional Transport in a Plasma with Steep Gradients; June 1999

NIFS-602 T. Mutoh, R. Kumazawa, T. Saki, K. Saito, F. Simpo, G. Nomura, T. Watari, X. Jikang, G. Cattanei, H. Okada, K. Ohkubo, M. Sato, S. Kubo, T. Shimozuma, H. Idei, Y. Yoshimura, O. Kaneko, Y. Takeiri, M. Osakabe, Y. Oka, K. Tsumori, A. Komori, H. Yamada, K. Watanabe, S. Sakakibara, M. Shoji, R. Sakamoto, S. Inagaki, J. Miyazawa, S. Morita, K. Tanaka, B.J. Peterson, S. Murakami, T. Minami, S. Ohdachi, S. Kado, K. Narihara, H. Sasao, H. Suzuki, K. Kawahata, N. Ohyabu, Y. Nakamura, H. Funaba, S. Masuzaki, S. Muto, K. Sato, T. Morisaki, S. Sudo, Y. Nagayama, T. Watanabe, M. Sasao, K. Ida, N. Noda, K. Yamazaki, K. Akaishi, A. Sagara, K. Nishimura, T. Ozaki, K. Toi, O. Motojima, M. Fujiwara, A. Iiyoshi and LHD Exp. Group 1 and 2,
First ICRF Heating Experiment in the Large Helical Device; July 1999

NIFS-603 P.C. de Vries, Y. Nagayama, K. Kawahata, S. Inagaki, H. Sasao and K. Nagasaki,
Polarization of Electron Cyclotron Emission Spectra in LHD, July 1999

NIFS-604 W. Wang, N. Nakajima, M. Okamoto and S. Murakami,
δf Simulation of Ion Neoclassical Transport; July 1999

NIFS-605 T. Hayashi, N. Mizuguchi, T. Sato and the Complexity Simulation Group,
Numerical Simulation of Internal Reconnection Event in Spherical Tokamak, July 1999

NIFS-606 M. Okamoto, N. Nakajima and W. Wang,
On the Two Weighting Scheme for δf Collisional Transport Simulation, Aug. 1999

NIFS-607 O. Motojima, A.A. Shishkin, S. Inagaki, K.Y. Watanabe,
Possible Control Scenario of Radial Electric Field by Loss-Cone-Particle Injection into Helical Device, Aug. 1999

NIFS-608 R. Tanaka, T. Nakamura and T. Yabe,
Constructing Exactly Conservative Scheme in Non-conservative Form, Aug. 1999

NIFS-609 H. Sugama,

Gyrokinetic Field Theory; Aug. 1999

NIFS-610 M. Takechi, G. Matsunaga, S. Takagi, K.Ohkuni, K. Toi, M. Osakabe, M. Isobe, S. Okamura, K. Matsuoka, A. Fujisawa, H. Iguchi, S. Lee, T. Minami, K. Tanaka, Y. Yoshimura and CHS Group,
Core Localized Toroidal Alfven Eigenmodes Destabilized By Energetic Ions in the CHS Heliotron/Torsatron, Sep. 1999

NIFS-611 K. Ichiguchi,
MHD Equilibrium and Stability in Heliotron Plasmas; Sep. 1999

NIFS-612 Y. Sato, M. Yokoyama, M. Wakatani and V. D. Pusovitov,
Complete Suppression of Pfirsch-Schluter Current in a Toroidal l=3 Stellarator; Oct. 1999

NIFS-613 S. Wang, H. Sanuki and H. Sugama,
Reduced Drift Kinetic Equation for Neoclassical Transport of Helical Plasmas in Ultra-low Collisionality Regime, Oct. 1999

NIFS-614 J. Miyazawa, H. Yamada, K. Yasui, S. Kato, N., Fukumoto, M. Nagata and T. Uyama,
Design of Spheromak Injector Using Conical Accelerator for Large Helical Device; Nov. 1999

NIFS-615 M. Uchida, A. Fukuyama, K. Itoh, S.-I. Itoh and M. Yagi,
Analysis of Current Diffusive Ballooning Mode in Tokamaks; Dec. 1999

NIFS-616 M. Tanaka, A.Yu Grosberg and T Tanaka,
Condensation and Swelling Behavior of Randomly Charged Multichain Polymers by Molecular Dynamics Simulations; Dec. 1999

NIFS-617 S. Goto and S. Kida,
Sparseness of Nonlinear Coupling, Dec. 1999

NIFS-618 M.M. Skoric, T. Sato, A. Maluckov and M.S. Jovanovic,
; *Complexity in Laser Plasma Instabilities* Dec. 1999

NIFS-619 T.-H. Watanabe, H. Sugama and T. Sato,
Non-dissipative Kinetic Simulation and Analytical Solution of Three-mode Equations of Ion Temperature Gradient Instability; Dec. 1999

NIFS-620 Y. Oka, Y. Takeiri, Yu.I.Belchenko, M. Hamabe, O. Kaneko, K. Tsumori, M. Osakabe, E. Asano, T. Kawamoto, R. Akiyama,
Optimization of Cs Deposition in the 1/3 Scale Hydrogen Negative Ion Source for LHD-NBI System ;Dec. 1999

NIFS-621 Yu.I. Belchenko, Y. Oka, O. Kaneko, Y. Takeiri, A. Krivenko, M. Osakabe, K. Tsumori, E. Asano, T. Kawamoto, R. Akiyama,
Recovery of Cesium in the Hydrogen Negative Ion Sources; Dec. 1999

NIFS-622 Y. Oka, O. Kaneko, K. Tsumori, Y. Takeiri, M. Osakabe, T. Kawamoto, E. Asano, and R. Akiyama,
H- Ion Source Using a Localized Virtual Magnetic Filter in the Plasma Electrode: Type I LV Magnetic Filter: Dec 1999

NIFS-623 M. Tanaka, S Kida, S. Yanase and G. Kawahara,
Zero-absolute-vorticity State in a Rotating Turbulent Shear Flow, Jan. 2000

NIFS-624 F. Leuterer, S. Kubo,
Electron Cyclotron Current Drive at $\omega \approx \omega_c$ with X-mode Launched from the Low Field Side; Feb 2000

NIFS-625 K. Nishimura,
Wakefield of a Charged Particulate Influenced by Emission Process of Secondary Electrons; Mar. 2000

NIFS-626 K. Itoh, M. Yagi, S.-I. Itoh, A. Fukuyama,
On Turbulent Transport in Burning Plasmas; Mar. 2000

NIFS-627 K. Itoh, S.-I. Itoh, L. Giannone,
Modelling of Density Limit Phenomena in Toroidal Helical Plasmas; Mar. 2000